Protrusion of Cu-TSV under different strain states

Jinxin Liu[1], Zhiheng Huang[1]*, Paul Conway[2], and Yang Liu[3]*

[1]School of Materials Science and Engineering, Sun Yat-sen University, Guangzhou 510275, China

[2]School of Mechanical, Electrical and Manufacturing Engineering, Loughborough University, Loughborough LE11 3TU, UK

[3]School of Electronics and Information Technology, Sun Yat-sen University, Guangzhou 510006, China

*email: hzh29@mail.sysu.edu.cn (Z. Huang), liuy69@mail.sysu.edu.cn (Y. Liu)

Abstract

A phase-field-crystal (PFC) model is used to investigate the protrusion of blind TSVs under different strain states. The direction of loading applied to the TSVs has an effect on the protrusion, which is closely related to the copper grains and their orientations at the TSV edges. A nonlinear relation between protrusion and strain rate has been found, which can be explained by different mechanisms of deformation. A higher strain occurring near the top end of the TSVs leads to a larger protrusion of the bind TSVs.

1. Introduction

The semiconductor industry aims for smaller, lighter and higher-performance products. Nowadays, the planar scaling of the two-dimensional (2D) semiconductor devices based on the Moore's law has reached its limit and how to overcome this barrier is becoming an urgent topic. The next generation packaging technology is expected to keep up with the increasing requirement of package density by using there-dimensional (3D) system integration. Chip stacking in vertical direction brings benefits of smaller form factor, shorter interconnection, and more functionality. In realizing 3D system integration, an important idea is to utilize through-silicon-via (TSV) technology [1]. The normal filler material used in TSV is copper, due to the low resistivity and the availability of a mature electro-plating process for deep trench filling [2]. However, the mismatch of coefficient of thermal expansion between copper and the surrounding silicon frequently leads to protrusion when the TSV structures are subjected to thermal processing [3-5]. This causes the damage of back-end-of-line (BEoL) layers and thus the failure of 3D packaging, posing a serious reliability problem to be solved.

Meanwhile, the packaging materials are approaching the nano-scale. As an example, nanowires have been considered as interconnects in future nano-devices [6]. IMEC has also proposed a new program called advanced nano-interconnection, to meet the severe demands of performance of advanced interconnects [7]. As the dimension of the packaging materials scales down, the material microstructure is becoming a more and more salient factor, especially considering its random and statistical nature [4]. There exist a few studies aiming for relating the microstructural factor to the copper protrusion of TSVs. An electron back-scattered diffraction (EBSD) technique used by Jiang *et al.* revealed the grain growth process of polycrystalline copper during thermal cycling [3]. Messemaeker *et al.* established a statistical model linking the protrusion height and the microstructure via studying a large ensemble of TSV protrusions [4].

To provide better understanding of the root cause of copper TSV protrusion, the strain or stress state presenting in the TSVs needs to be determined. There are a few experimental studies attempting to analyze the stress in the TSVs. Nano-indentation is used by Che *et al.* to measure the residual stress in the TSV [8]. Okoro *et al.* measured the stress of the TSVs of different diameters using a micro-Raman spectroscopy [9]. Liu *et al.* used synchrotron X-ray microdiffraction to measure the microscale thermomechanical strain in-situ [10]. As a supplement, simulation on TSV protrusion considering the microstructure can provide more details. In a recent work, we reproduced the process of copper protrusion of TSV using a phase-field-crystal (PFC) model, revealing the microstructural evolution at the atomic scale [11].

In this study, we investigate the protrusion behavior of the TSV under different strain states. The remainder of this paper is organized as follows. First, the PFC method is briefly reviewed. Then, different strain states applied to the TSV structures are discussed. Different kinds of strain states are studied, including the directions of loading, the strain rate and the distributions of strain along the edges of TSV.

2. Methods

In PFC model, the lattice of a crystalline material is represented as an order parameter ρ. The order parameter represents the local time-averaged atomic density of a material system. In addition, developed by Wu *et al.*, a two-point correlation function is introduced, and the corresponding two-model PFC model is used to simulate a square lattice in two dimensions [12]. In the 2D case, the two-mode order parameter is written as [12]:

$$\rho = \bar{\rho} + A[\cos(qx) + \cos(qy)] + B\cos(qx)\cos(qy) \quad (1)$$

where $\bar{\rho}$ is the average density. A and B are related to the amplitudes of two sets of density waves. q is a parameter related to the lattice constant, hereinafter referred to as $a \approx 0.25nm$, with the relationship $q = 2\pi/a$. In the 2D simulation, a square lattice corresponds to the {100} crystallographic plane of copper. Then, the free energy of the material system is written as [12]:

$$F[\rho] = \int \mathrm{d}\vec{r}\left\{\frac{\rho}{2}[r + (\nabla^2 + 1)^2(\nabla^2 + Q^2)^2]\rho + \frac{\rho^4}{4}\right\} \quad (2)$$

where r is the scaling temperature and $Q^2 = 2$ is a constant. Finally, the evolution of the microstructure is given by solving the governing equation of the PFC model [12]:

$$\frac{\partial \rho}{\partial t} = \nabla^2 \frac{\delta F}{\delta \rho} \quad (3).$$

The model configuration of our TSV structure is shown in Fig. 1. The solid gray lines mark out the edges of the TSV, showing a trapezoid TSV. Note that the TSV is a blind via in this study. To mimics mechanical loading to the TSVs, we used the technique introduced by Stefanovic *et al.* in [13]. Solid external layers are added to surround the TSV manually. The top layer of TSV is set as the lattice with a 0° orientation and serves as a solid cover. Moreover, the grain orientations of other external layers are adjusted to accommodate the corresponding grains at both edges of the TSV. In the PFC model, the free energy is modified by adding a "penalty term" with the form:

$$F[\rho]' = F[\rho] + \int \mathrm{d}\vec{r}\, M(\vec{r})[\rho(\vec{r},t) - \rho(\vec{r}(\vec{v},t),t)] \quad (4)$$

where $M(\vec{r})$ is nonzero only in the external layers, except for the top cover layer. With the "penalty term" applied, the atoms inside the external layers are motivated to move with a

predetermined velocity $\vec{v}$ in a direction defined by the arrows, forming an angle θ with the horizontal line, as demonstrated in Fig. 1. Therefore, the "penalty term" mimics the effect of a compressive strain applied to the TSV. The parameters in our PFC model are setting as $(r, \bar{\rho}, A, B, q, |\vec{v}|, \theta) = (-1, 0.59, -0.31, -0.14, 1.0, 1.0 \times 10^{-3}, 120°)$ unless otherwise specified. Note that the length and time scales in this study are dimensionless. In addition, the atoms in or near the GBs and dislocations in the TSV are defined as defect atoms, as highlighted by the brighter dots in Fig. 1.

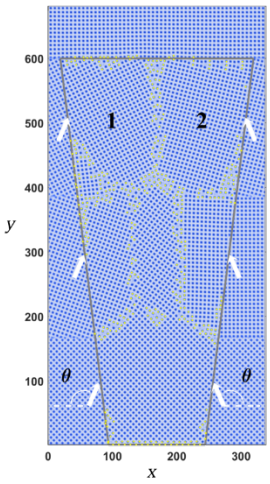

Fig. 1 The model configuration of a TSV structure. The solid gray lines mark out the edges of a trapezoid TSV. The parallel arrows form an angle θ with the horizontal line, which indicate the strain applied to the TSV. The defect atoms in the TSV are highlighted by the brighter dots. Note that the length scales in *x* and *y* direction are dimensionless.

3. Results and Discussion

3.1 The direction of loading

To simulate a TSV under different strain states, the direction of loading θ is changed systematically from $90°$ to $240°$, which represents all the scenarios of the strain states that the TSV could be subjected to. For example, the strain with $\theta = 180°$ means a pure compressive strain to the TSV, while the strain with $\theta = 150°$ represents the combination of a compressive strain and a shear strain. Fig. 2 shows the protrusion of three TSVs with different loadings, i.e., $\theta = 180°, 150°$ and $120°$. The protrusions of TSVs at the time *t* = 30000 of the loading stage are sketched by the black dashed curves. It can be seen that the maximal protrusion is the largest for the second TSV. Moreover, the relationship between the TSV protrusion and the direction of loading is plotted in Fig. 3a. The curves show that the protrusion increases then decreases with the increasing θ in general, with the maximal mean protrusion occurring at $\theta = 135°$.

A stress-driven interfacial sliding model proposed by Kumar *et al.* was used to predict the protrusion height [14]. But in this model, the microstructural effect was not considered. Next, we will show how the protrusion is influenced by the grain orientation and the direction of loading. For the case discussed above, the orientations of the grains in the top end of the TSVs, labelled with grain 1 and 2, are $28°$ and $70°$ respectively, as shown in Fig. 1. The protrusion of grain 1 and 2 are measured and plotted in Fig. 3b. It can be seen that for grain 1, the largest protrusion is caused by the strain with a $\theta = 150°$, while for grain 2 $\theta = 120°$. Meanwhile, the protrusion of grain 2 is larger than grain 1 for the θ within the range $[90°, 180°]$. This demonstrates the fact that the protrusion is related to the grain orientation. A smaller difference between the grain orientation and the direction of loading, i.e., θ, will lead to a higher protrusion. This effect can be significantly important when the TSV scaling is reduced into the nanometer regime where only a few grains exist in the TSV.

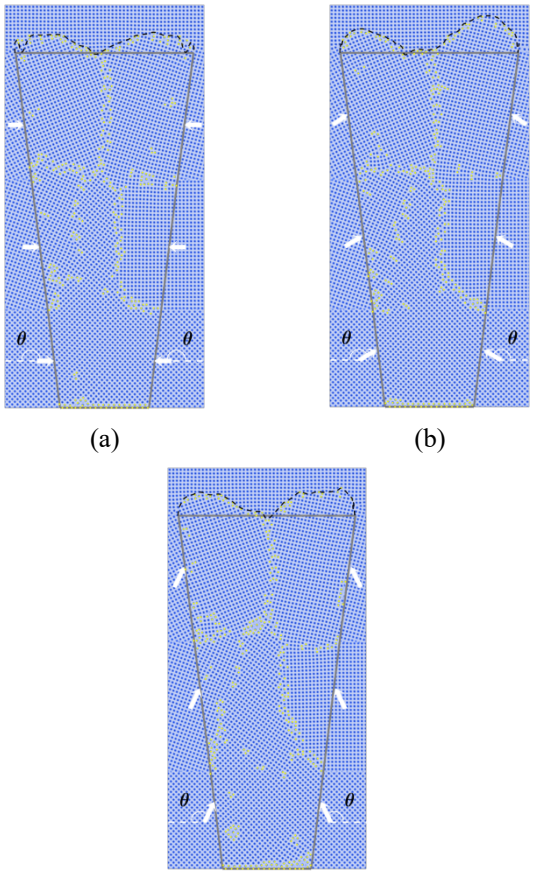

(a) (b)

(c)

Fig. 2 Three TSVs are applied with different direction of loading: (a) $\theta = 180°$, (b) $\theta = 150°$, and (c) $\theta = 120°$. The black dashed curves mark out the protrusion at time *t* = 30000 of the loading stage.

3.2 The effect of strain rate

The strain rate applied to the TSV also influences the protrusion behavior. In this study, the parameter $|\vec{v}|$ is corresponding to the strain rate. Note that $|\vec{v}|$ is dimensionless because the time and length in the PFC model are dimensionless. With the same initial microstructure, the TSVs are applied with different strain rate from 4×10^{-4} to 20×10^{-4}. The mean protrusion under different conditions is plotted in Fig. 4a. It shows that the protrusion is dependent on the strain rate. The largest protrusion occurs under the strain rate 8×10^{-4}. The protrusion firstly increases with increasing the strain rate until 8×10^{-4}, then decreases and finally hardly increases within the range from 10×10^{-4} to 20×10^{-4}. Furthermore, the protrusion vs. the applied strain under different strain rate is plotted in Fig. 4b. The rates of protrusion under four different strain rates are almost the same at the beginning. But the protrusion does not substantially increase after $\varepsilon = 5\%$ under the strain rates 4×10^{-4}, 12×10^{-4}, and 16×10^{-4}, while keep increasing under the strain rate

8×10^{-4}. This leads to a much higher protrusion under the strain rate 8×10^{-4}. The effect of the strain rate on TSV protrusion may be explained by different mechanisms of deformation. Under a lower strain rate, the creep behavior of the grains is dominant. The dislocation motion is only activated under a higher strain rate [15]. A more active dislocation motion under a higher strain rate is also observed in our previous simulation [11]. Therefore, the relief of strain under a higher strain rate can be achieved through dislocation motion and results in a lower protrusion of the TSV. When the dimension of the TSV approaches the nanoscale, the strain rate sensitivity of the strength of nano-copper is becoming more obvious than the coarse-grain copper [16]. To adjust the strain rate applied to the TSV, controlling the rate of heating during thermal processing could be a solution. For example, Kumar *et al.* reported that a slow heating rate led to a higher protrusion [14]. This shows a similar tendency to the strain rate during 8×10^{-4} to 14×10^{-4} in our simulation.

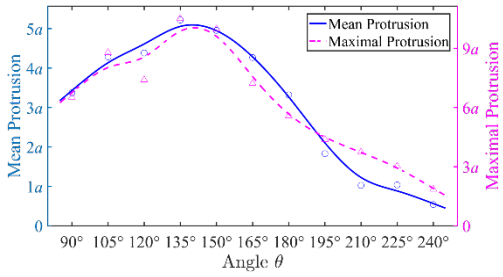

(a)

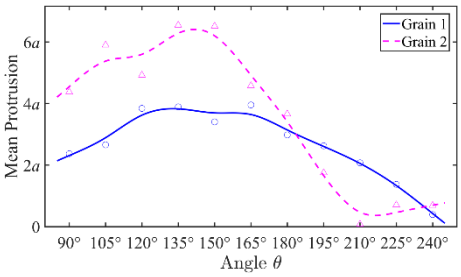

(b)

Fig. 3 (a) The plot of protrusion verses the direction of loading θ. The mean and maximal protrusion height are plotted by solid and dashed curve, respectively. (b) The mean protrusion caused by grains 1 and 2 under different strain applied.

3.3 The strain distributions

As discussed above, the applied strains are uniform along the edges of the TSVs. Next, we will study the cases of ununiform strain with simple distributions along the edges of the TSV. The strain distributions are controlled by varying the strain rate $|\vec{v}|$ in different regions of the edges. The model settings are summarized in Table. 1, and the corresponding results are shown in Fig. 5. Firstly, comparing M2 with M3, the protrusion is almost the same for the two TSVs, which suggests that the strain variation at the bottom region has little effect on protrusion. Then, comparing M3 with the TSV shown in Fig. 2c, the protrusion is also similar. Finally, when examining M1 and M4, it is observed that the protrusion is much smaller comparing with other TSVs. This suggests that the strain applied near the top end of the TSV has a greater effect on protrusion. In addition, with a larger strain applied, a larger protrusion will be resulted. An experimental work also suggested that the local strain near the top end of TSV may be responsible for the protrusion from the observation that a TSV with a higher protrusion is subjected to a higher strain near the top end of the TSV [16].

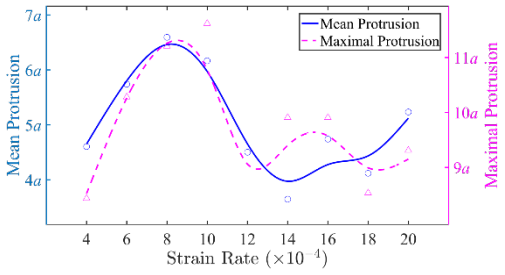

(a)

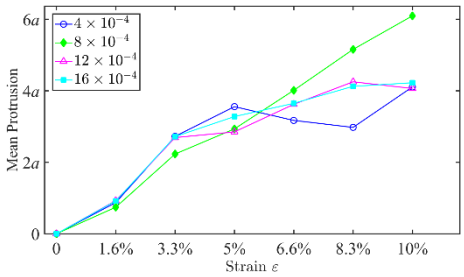

(b)

Fig. 4 (a) The plot of protrusion vs. the strain rate from 4×10^{-4} to 20×10^{-4}. The mean and maximal protrusion height are plotted by solid and dashed curve, respectively. (b) The mean protrusion height to the strain with four different strain rates applied are plotted.

Table 1. The strain distribution in different regions. The coordinate of TSV is illustrated in Fig. 1 and Fig. 5.

	Strain rate applied in different regions		
Model No.	$600 \geq y \geq 350$	$350 \geq y \geq 130$	$130 \geq y \geq 0$
M1	1×10^{-4}	5×10^{-4}	10×10^{-4}
M2	10×10^{-4}	5×10^{-4}	1×10^{-4}
M3	10×10^{-4}	5×10^{-4}	10×10^{-4}
M4	5×10^{-4}	10×10^{-4}	5×10^{-4}

4. Conclusions

In this paper, a two-mode PFC model is utilized to simulate the protrusion of blind Cu-TSVs. The effects of different strain states on protrusion are studied. It can be concluded that:

1) The direction of loading applied to the TSVs has an effect on protrusion, which is closely related to the grains and their orientation at the edges.
2) The protrusion is found to have a nonlinear relationship with strain rate and the largest protrusion is produced under $|\vec{v}| = 8 \times 10^{-4}$.
3) The distribution of strain along the TSV edges also influences the protrusion. The strain applied at the bottom edge of the TSVs has little effect on protrusion. A higher strain applied near the top end of the TSV leads to a larger protrusion out of the blind TSVs.

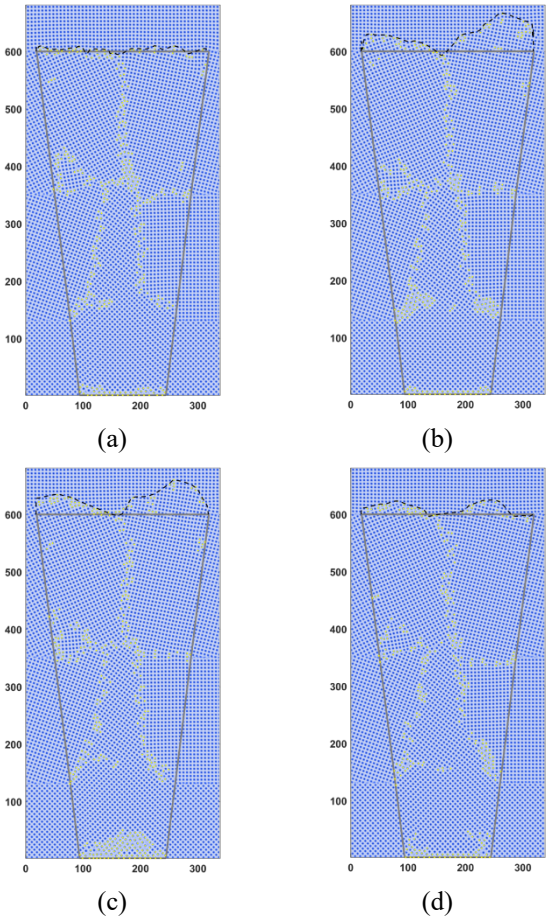

Fig. 5 TSVs with different distribution of strain along the edges. The corresponding models are (a) M1, (b) M2, (c) M3, and (d) M4 summarized in Table 1. The black dashed curves sketch the protrusion profile at t = 30000.

Acknowledgments

The authors acknowledge financial support from the National Natural Science Foundation of China (NSFC) under grants 51832002, the Guangdong Natural Science Foundation under grant 2015A030312011, and the Zhuhai Key Technology Laboratory of Wide Bandgap Semiconductor Power Electronics under grant 20167612042080001.

References

1. M. M. Shulaker, G. Hills, R. S. Park, R. T. Howe, K. Saraswat, H. S. P. Wong, and S. Mitra, "Three-dimensional integration of nanotechnologies for computing and data storage on a single chip," Nature, vol. 547, pp. 74–78, Jul. 2017.

2. C.-F. Hsu, W.-P. Dow, H.-C. Chang, and W.-Y. Chiu, "Optimization of the copper plating process using the taguchi experimental design method i. microvia filling by copper plating using dual levelers," Journal of The Electrochemical Society, vol. 162, no. 10, pp. D525–D530, 2015.

3. T. Jiang, J. Im, R. Huang, and P. S. Ho, "Through-silicon via stress characteristics and reliability impact on 3D integrated circuits," MRS Bulletin, vol. 40, no. 3, pp. 248–256, Mar. 2015.

4. J. D. Messemaeker, P. J. Roussel, O. V. Pedreira, T. V. der Donck, S. V. Huylenbroeck, E. Beyne, I. D. Wolf, M. Stucchi, and K. Croes, "Statistical distribution of through-silicon via Cu pumping," IEEE Transactions on Device and Materials Reliability, vol. 17, no. 3, pp. 549–559, Sep. 2017.

5. C. Okoro, L. E. Levine, R. Xu, and Y. S. Obeng, "Experimentally, how does Cu TSV diameter influence its stress state?" in 2015 IEEE 65th Electronic Components and Technology Conference (ECTC), San Diego, CA, USA, May 2015, pp. 54–58.

6. W. H. Xu, L. Wang, Z. Guo, X. Chen, J. Liu, and X. J. Huang, "Copper nanowires as nanoscale interconnects: Their stability, electrical transport, and mechanical properties," ACS Nano, vol. 9, no. 1, pp. 241–250, Jan. 2015.

7. G. Murdoch, J. Bmmels, C. J. Wilson, K. B. Gavan, Q. T. Le, Z. Tkei, and W. Clark, "Feasibility study of fully self aligned vias for 5nm node BEOL," in 2017 IEEE International Interconnect Technology Conference (IITC), Hsinchu, Taiwan, May 2017, pp. 1–4.

8. F. X. Che, W. N. Putra, A. Heryanto, A. Trigg, X. Zhang, and C. L. Gan, "Study on Cu protrusion of through-silicon via," IEEE Transactions on Components, Packaging and Manufacturing Technology, vol. 3, no. 5, pp. 732–739, May 2013.

9. C. Okoro, Y. Yang, B. Vandevelde, B. Swinnen, D. Vandepitte, B. Verlinden, and I. de Wolf, "Extraction of the appropriate material property for realistic modeling of through-silicon-vias using micro-Raman spectroscopy," in 2008 International Interconnect Technology Conference, June 2008, pp. 16–18.

10. X. Liu, P. A. Thadesar, C. L. Taylor, H. Oh, M. Kunz, N. Tamura, M. S. Bakir, and S. K. Sitaraman, "In-situ microscale through-silicon via strain measurements by synchrotron x-ray microdiffraction exploring the physics behind data interpretation," Applied Physics Letters, vol. 105, no. 11, p. 112109, Sep. 2014.

11. J. Liu, Z. Huang, P. P. Conway, F. Altmann, M. Petzold, and F. Naumann, "On reproducing the copper extrusion of through-silicon-vias from the atomic scale," in 2017 18th International Conference on Electronic Packaging Technology (ICEPT), Harbin, China, Aug. 2017, p. 789–796.

12. K. A. Wu, A. Adland, and A. Karma, "Phase-field-crystal model for fcc ordering," Physical Review E, Vol. 81, p. 061601, Jun. 2010.

13. P. Stefanovic, M. Haataja, and N. Provatas, "Phase field crystal study of deformation and plasticity in nanocrystalline materials," Physical Review E, Vol. 80, p. 046107, Oct. 2009.

14. P. Kumar, I. Dutta, and M. Bakir, "Interfacial effects during thermal cycling of cu-filled through-silicon vias (tsv)," Journal of electronic materials, vol. 41, no. 2, pp. 322–335, 2012.

15. Y. Wang and E. Ma, "Temperature and strain rate effects on the strength and ductility of nanostructured copper," Applied physics letters, vol. 83, no. 15, pp. 3165–3167, 2003.

16. T. Jiang, C. Wu, L. Spinella, J. Im, N. Tamura, M. Kunz, H.-Y. Son, B. G. Kim, R. Huang, and P. S. Ho, "Plasticity mechanism for copper extrusion in through-silicon vias for three-dimensional interconnects," Applied Physics Letters, vol. 103, no. 21, p. 211906, Nov. 2013.